Supplementary Information (SI) for New Journal of Chemistry.
This journal is © The Royal Society of Chemistry and the Centre National de la Recherche Scientifique 2026
Supplementary Information (SI) for New Journal of Chemistry.
This journal is © The Royal Society of Chemistry and the Centre National de la Recherche Scientifique 2025

Supplementary Information

Mixed-phase $FeMoO_4$ for synergistic photocatalytic peroxydisulfate activation toward efficient tetracycline degradation

Runyu Cai,†[a] Zhongliang Shi,†[a] Shifeng Li,[a] Shuhua Yao,[a] Dongjing Wang,[a] Man Xu*[ab] and Xuan Cao*[c]

[a]*College of science, Shenyang University of Chemical Technology, Shenyang, Liaoning, 110142, China*

[b]*Instrumental Analysis Center, Shenyang University of Chemical Technology, Shenyang, Liaoning, 110142, China. E-mail: xuman.jlu@vip.163.com*

[c]*Center for Interdisciplinary Research and Innovation, Muyuan Laboratory, Zhengzhou, Henan, 450016, China. E-mail: cx.1988@aliyun.com*

† These two authors contributed equally to this paper.

CONTENT

Text S1. Materials.

Methanol (MeOH, > 99.7%), ethanol (EtOH, > 99.7%) and sodium bicarbonate ($NaHCO_3$, > 99.5%) were obtained from Tianjin Yongda Chemical Reagent Co., Ltd. tert-Butanol (t-BuOH, > 99.5%), sodium chloride (NaCl, > 99.5%), sodium nitrate ($NaNO_3$, > 99%), disodium hydrogen phosphate dodecahydrate ($Na_2HPO_4{\cdot}12H_2O$, > 99%), sodium dihydrogen phosphate dodecahydrate ($NaH_2PO_4{\cdot}12H_2O$, > 99%), and sodium sulfate (Na_2SO_4, > 99%) were supplied by Tianjin Damao Chemical Reagent Co., Ltd. Sodium hydroxide (NaOH, > 96%) was provided by Tianjin Hengxing Chemical Reagent Manufacturing Co., Ltd. Ferrous sulfate heptahydrate ($FeSO_4{\cdot}7H_2O$, > 99%), sodium molybdate dihydrate ($Na_2MoO_4{\cdot}2H_2O$, > 99%), hydrochloric acid (HCl, 36–38%), TC hydrochloride ($C_{22}H_{24}N_2O_8{\cdot}HCl$, > 98%), p-benzoquinone ($C_6H_4O_2$, > 98%), isopropanol (i-PrOH, > 99.7%), and sodium carbonate (Na_2CO_3, > 99.8%) were purchased from Sinopharm Chemical Reagent Co., Ltd. L-Histidine ($C_6H_9N_3O_2$, > 99%) was acquired from Macklin Biochemical Technology Co., Ltd., and sodium persulfate ($Na_2S_2O_8$, > 99%) was sourced from Shanghai Aladdin Biochemical Technology Co., Ltd.

Text S2. Characterization.

The powder X-ray diffraction (XRD) measurements were performed using a D8 Advance Bruker X-ray diffractometer, utilizing Cu Kα radiation (λ = 0.5418 nm) under conditions of 56 KV and 182 mA. To observe morphology and perform element mapping analysis, a scanning electron microscope (SEM-JSM-6360LV) equipped with energy dispersive X-ray spectroscopy (EDX-S-3400N) was utilized. The structural and morphological features of the nanoparticles were observed using a high-resolution transmission electron microscope (JEM-F200, Japan, TEM). The functional groups and chemical structure of the prepared catalyst samples were analyzed using the IRTracer-100 Fourier Transform Infrared Spectrometer (FT-IR) produced by Shimadzu Corporation of Japan. Specific surface areas were determined using a BELSORP-miniX analyzer through N_2 adsorption-desorption, applying the Brunauer-Emmett-Teller (BET) and Barrett-Joyner-Halenda (BJH) methods. The chemical composition and valence states of the samples were analyzed using X-ray Photoelectron Spectroscopy (XPS-Thermo ESCALAB 250), with further investigation into

the charge transfer pathway. Additionally, the spectra were calibrated relative to the C 1s peak at 284.8 eV. The optical adsorption capacity of the catalysts was assessed using the Hitachi U4100 UV spectrometer, operating within the spectral range of 190-900 nm. Photoluminescence (PL) spectra were obtained using a HORIBA spectrometer, with a monochromator slit width of 5.0 nm. Bruker E500 Electron Paramagnetic Resonance (EPR) spectroscopy was employed to detect active species.

Text S3. Photoelectrochemical measurements.

Electrochemical measurements were carried out on a CHI760E electrochemical workstation with a stand three-electrodes system. Among them, a Pt wire was used as the counter electrode, and the reference electrode was the saturated Ag/AgCl. The cleaned F-doped tin oxide (FTO) glass was used as the working electrode. 5 mg of corresponding photocatalyst and 20 μL of Nafion (5%) were added into 980 μL of ethanol to form a homogeneous slurry. The homogeneous slurry was ultrasonicated for 30 min and then coated on the FTO glass. The obtained system was dried at 150 °C for 60 min. The supporting electrolyte was Na_2SO_4 solution (0.5 M) with the pH value of 6.8. The incident visible light source was Xe lamp (300 W). The photocurrent-time was investigated in the irradiation of Xe lamp at a bias potential of 0.5 V vs. Ag/AgCl. The electrochemical impedance spectroscopy (EIS) was detected by an AC voltage amplitude of 10 mV at -0.3 V versus Ag/AgCl over the frequency range from 10 kHz to 0.01 Hz. The Mott-Schottky was studied in the electrolyte of Na_2SO_4 (0.5 M), and the frequency of the AC potential was set as 1000 Hz as well as the amplitude was 10 mV.

Text S4. Liquid chromatography-mass spectrometry test.

The intermediates generated during the decomposition of HTC were identified using liquid chromatography-mass spectrometry (LC-MS). A C18 column (4.6×150 nm) was employed with an injection volume of 10 μL, and eluent A consisted of 0.1% ammonium hydroxide (v/v), while acetonitrile served as eluent B. By combining 5% eluent A with 95% eluent B, effective separation could be achieved. Full-scan analysis in the range of 100 to 1500 m/z was conducted using electrospray ionization source in positive ionization mode (EIS(+)). The remaining operational parameters were set as follows: a capillary voltage of 4.5 kV, N_2 for desolvent gas, a gas temperature of 150 °C, and a gas flow rate of 15 L/min.

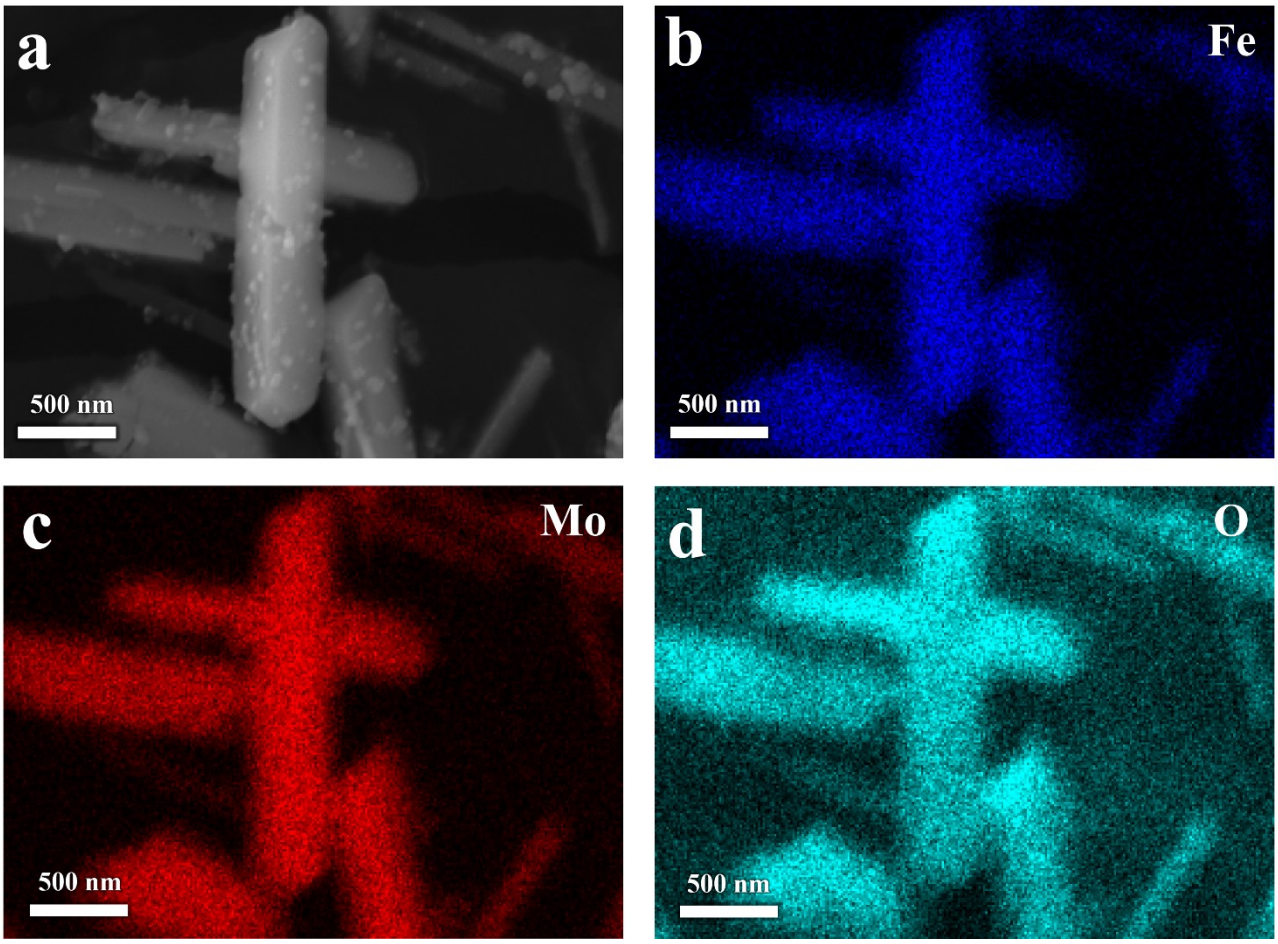

Fig. S1 SEM images of FeMoO4 (a). SEM-EDS mapping images of FeMoO4 (b-d).

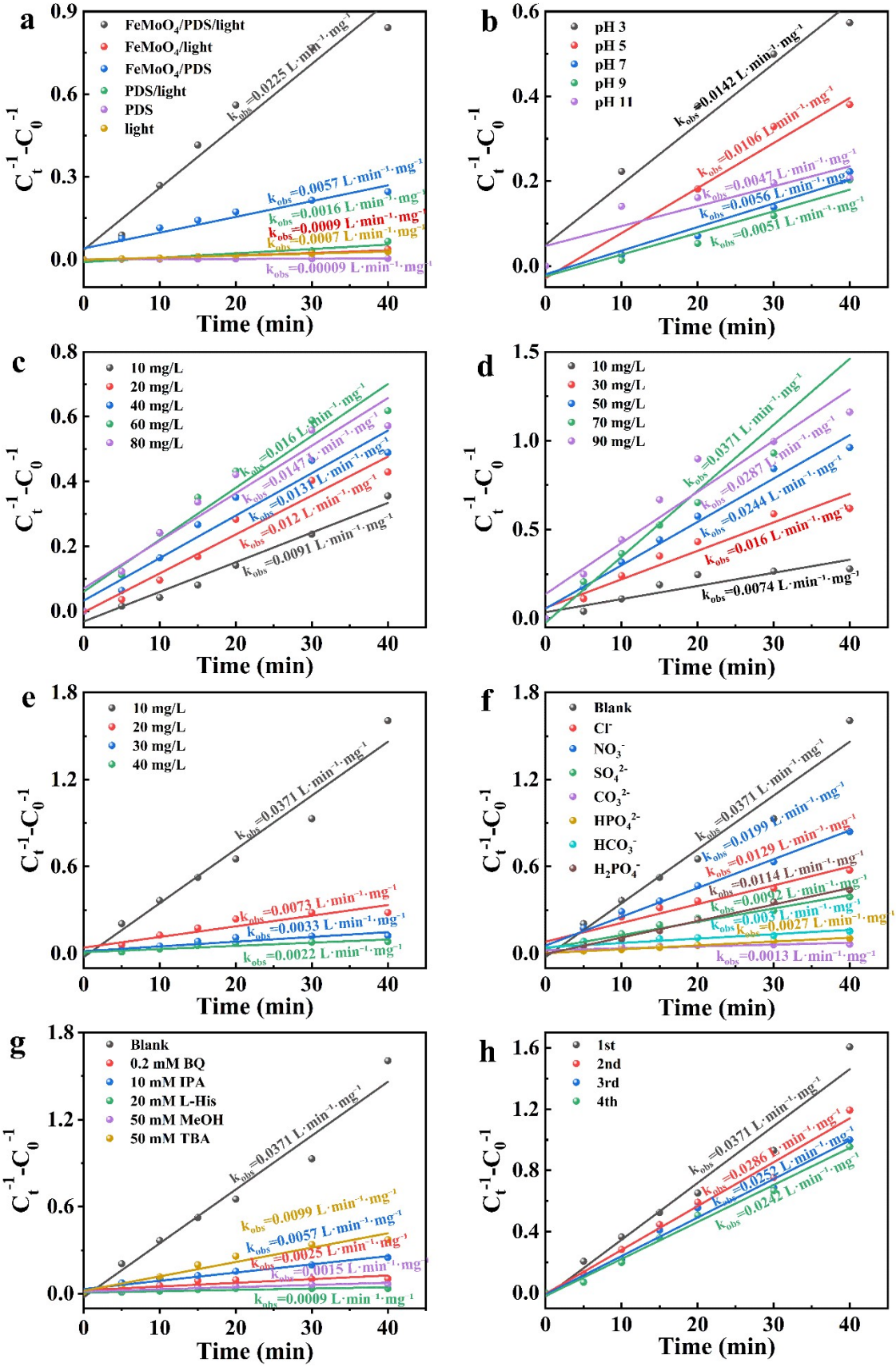

Fig. S2 Pseudo second-order kinetics models for different systems (a), solution pH (b), catalyst dosage (c), PDS dosage (d), TC concentration (e), Inorganic anions (f), scavengers (g), cycles (h). Reaction conditions: TC, 10 mg/L; pH, 3; $FeMoO_4$, 60 mg/L; PDS, 30 mg/L (a-c), 70 mg/L (d-h); anions, 10 mM (f).

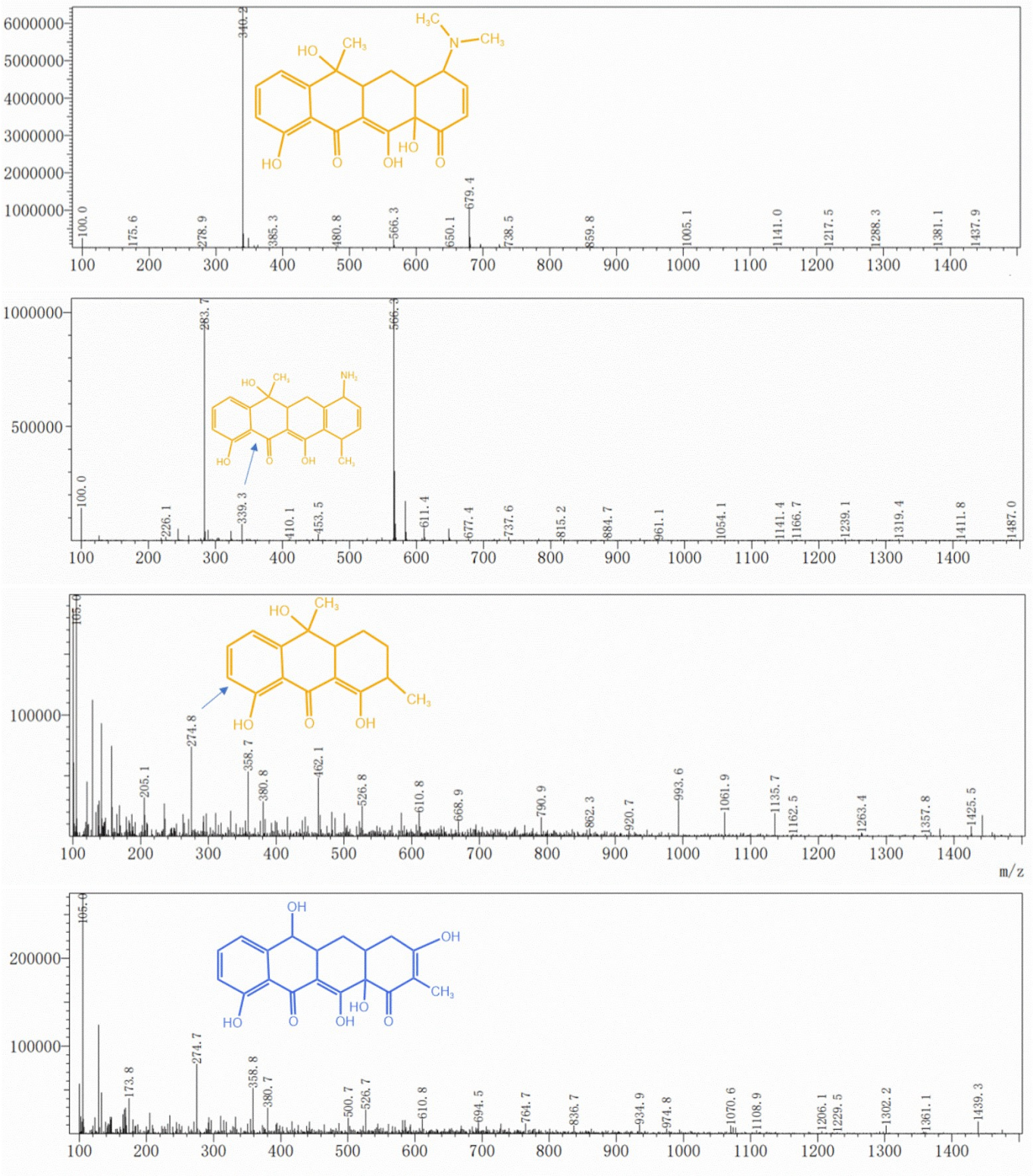
6000000
5000000
4000000
3000000
2000000
1000000
100.0
175.6
278.9
340.2
385.3
480.8
566.3
650.1
679.4
738.5
859.8
1005.1
1141.0
1217.5
1288.3
1381.1
1437.9
100
200
300
400
500
600
700
800
900
1000
1100
1200
1300
1400
HO
CH3
H3C
N
CH3
HO
HO
O
OH
O
1000000
500000
100.0
226.1
283.7
339.3
410.1
453.5
566.3
611.4
677.4
737.6
815.2
884.7
961.1
1054.1
1141.4
1166.7
1239.1
1319.4
1411.8
1487.0
NH2
CH3
100000
105.0
205.1
274.8
358.7
380.8
462.1
526.8
610.8
668.9
790.9
862.3
920.7
993.6
1061.9
1135.7
1162.5
1263.4
1357.8
1425.5
m/z
200000
105.0
173.8
274.7
358.8
380.7
500.7
526.7
610.8
694.5
764.7
836.7
934.9
974.8
1070.6
1108.9
1206.1
1229.5
1302.2
1361.1
1439.3
OH

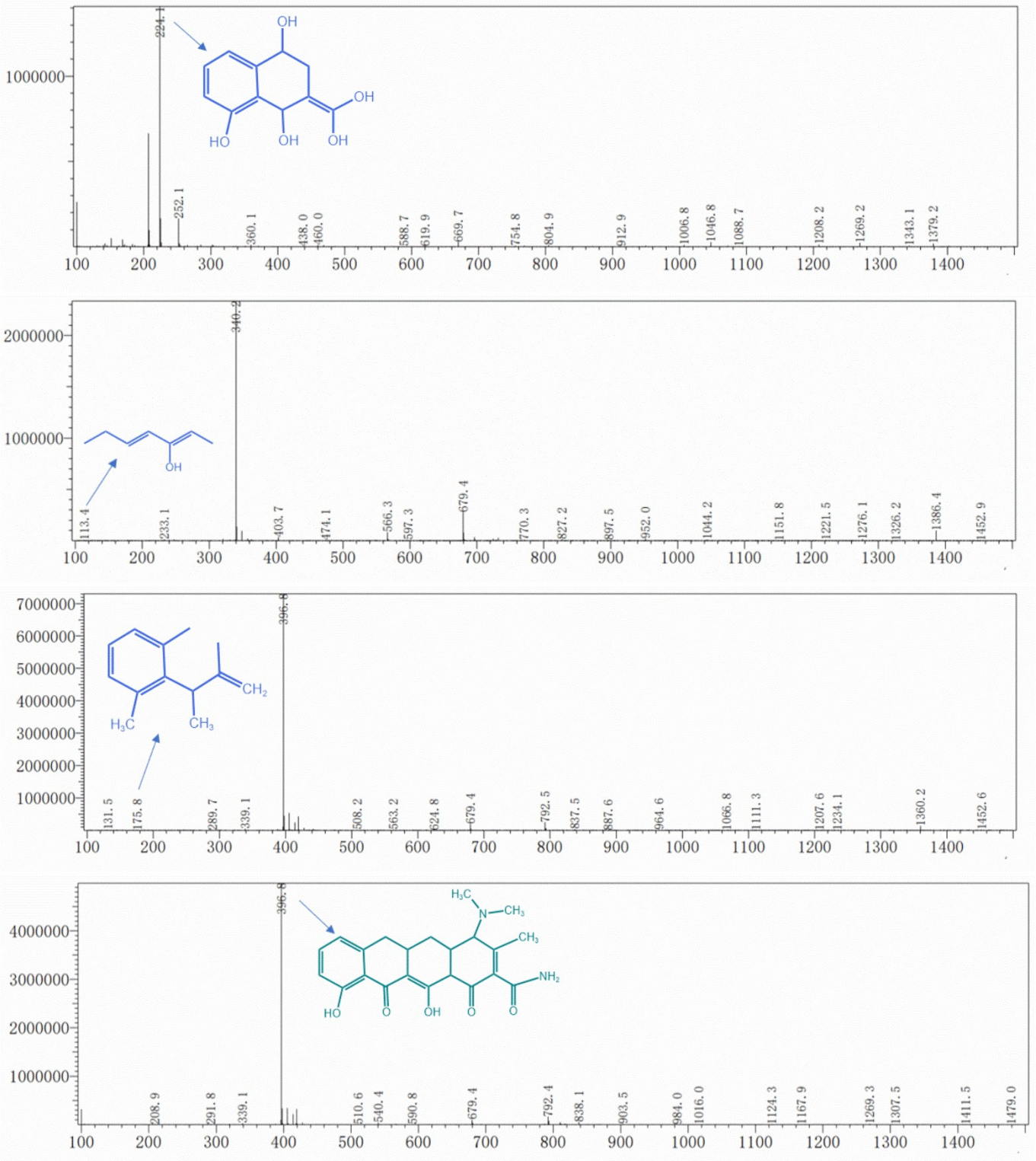
1000000
224.1
252.1
360.1
438.0
460.0
588.7
619.9
669.7
754.8
804.9
912.9
1006.8
1046.8
1088.7
1208.2
1269.2
1343.1
1379.2
OH
OH
HO
OH
OH
100 200 300 400 500 600 700 800 900 1000 1100 1200 1300 1400
2000000
1000000
340.2
113.4
233.1
403.7
474.1
566.3
597.3
679.4
770.3
827.2
897.5
952.0
1044.2
1151.8
1221.5
1276.1
1326.2
1386.4
1452.9
OH
100 200 300 400 500 600 700 800 900 1000 1100 1200 1300 1400
7000000
6000000
5000000
4000000
3000000
2000000
1000000
396.8
131.5
175.8
289.7
339.1
508.2
563.2
624.8
679.4
792.5
837.5
887.6
964.6
1066.8
1111.3
1207.6
1234.1
1360.2
1452.6
CH2
H3C
CH3
100 200 300 400 500 600 700 800 900 1000 1100 1200 1300 1400
4000000
3000000
2000000
1000000
396.8
208.9
291.8
339.1
510.6
540.4
590.8
679.4
792.4
838.1
903.5
984.0
1016.0
1124.3
1167.9
1269.3
1307.5
1411.5
1479.0
H3C
N
CH3
CH3
NH2
HO
O
OH
O
O
100 200 300 400 500 600 700 800 900 1000 1100 1200 1300 1400

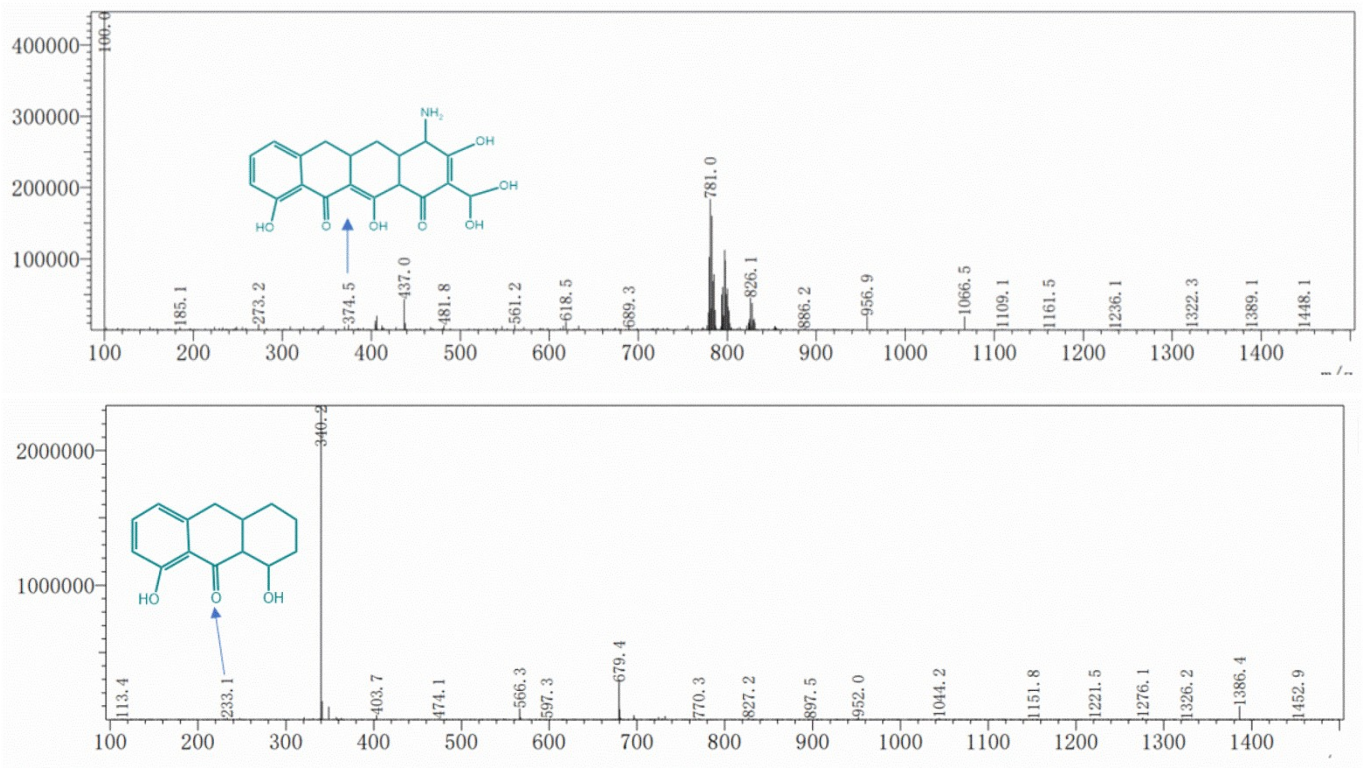

Fig. S3 LC-MS diagrams of TC degradation process.

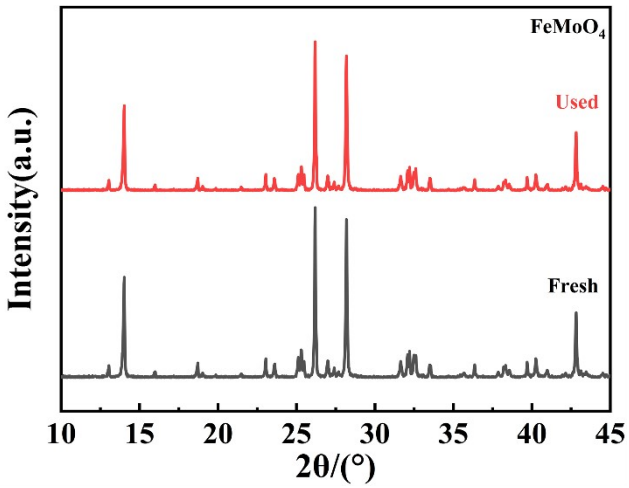

Fig. S4 Comparison of XRD patterns of $FeMoO_4$ before and after the reaction.

Table S1 Dynamic model fitting parameters of $FeMoO_4$, α-$FeMoO_4$, and β-$FeMoO_4$.

Sample	[PDS] (mg/L)	pH	[Cat] (mg/L)	[Pollution] (mg/L)	Pseudo first-order reaction		Pseudo second-order reaction	
					k_1 (min^{-1})	R^2	k_2(L·min^{-1}·mg^{-1})	R^2
α-$FeMoO_4$	30	3	60	10	0.0328	0.798	0.009	0.881
β-$FeMoO_4$	30	3	60	10	0.0306	0.814	0.0078	0.922
$FeMoO_4$	30	3	60	10	0.0428	0.804	0.016	0.941

Table S2 Dynamic model fitting parameters under different reaction conditions.

Visible light	[PDS] (mg/L)	pH	[Cat] (mg/L)	[Pollution] (mg/L)	Pseudo first-order reaction		Pseudo second-order reaction	
					k_1 (min^{-1})	R^2	k_2(L·min^{-1}·mg^{-1})	R^2
Yes	30	3	60	10	0.0513	0.835	0.0225	0.961
Yes	0	3	60	10	0.0069	0.966	0.0009	0.949
No	30	3	60	10	0.0246	0.809	0.0057	0.926
Yes	30	3	0	10	0.0118	0.914	0.0016	0.88
No	30	3	0	10	0.0008	0.988	8.6^{-5}	0.989
Yes	0	3	0	10	0.0065	0.989	0.0007	0.991

Table S3 Dynamic model fitting parameters under different pH and catalyst dose.

[PDS] (mg/L)	pH	[Cat] (mg/L)	[Pollution] (mg/L)	Pseudo first-order reaction		Pseudo second-order reaction	
				k_1 (min^{-1})	R^2	k_2(L·min^{-1}·mg^{-1})	R^2
30	3	60	10	0.0419	0.833	0.0142	0.963
30	5	60	10	0.0401	0.944	0.0106	0.957
30	7	60	10	0.0272	0.995	0.0056	0.958
30	9	60	10	0.0267	0.975	0.0051	0.928
30	11	60	10	0.0227	0.709	0.0047	0.798
30	3	10	10	0.0381	0.991	0.0091	0.976
30	3	20	10	0.042	0.91	0.012	0.958
30	3	40	10	0.0414	0.84	0.0131	0.941
30	3	60	10	0.0428	0.804	0.016	0.941
30	3	80	10	0.0402	0.785	0.0147	0.925

Table S4 Dynamic model fitting parameters under different PDS and TC concentration.

[PDS] (mg/L)	pH	[Cat] (mg/L)	[Pollution] (mg/L)	Pseudo first-order reaction		Pseudo second-order reaction	
				k_1 (min^{-1})	R^2	k_2(L·min^{-1}·mg^{-1})	R^2
10	3	60	10	0.0308	0.788	0.0074	0.856
30	3	60	10	0.0428	0.804	0.016	0.941
50	3	60	10	0.0501	0.823	0.0244	0.982
70	3	60	10	0.0585	0.872	0.0371	0.968
90	3	60	10	0.0514	0.729	0.0287	0.924
70	3	60	10	0.0585	0.872	0.0371	0.968
70	3	60	20	0.0413	0.75	0.0073	0.884
70	3	60	30	0.0362	0.767	0.0033	0.853
70	3	60	40	0.0341	0.795	0.0022	0.872

Table S5 Dynamic model fitting parameters under different Inorganic anions.

anions	[anions] (mM)	Pseudo first-order reaction		Pseudo second-order reaction	
		k_1 (min^{-1})	R^2	k_2(L·min^{-1}·mg^{-1})	R^2
Blank	0	0.0585	0.872	0.0371	0.968
Cl^-	10	0.0366	0.753	0.0129	0.943
NO_3^-	10	0.0451	0.824	0.0199	0.988
SO_4^{2-}	10	0.0327	0.858	0.0092	0.972
CO_3^{2-}	10	0.0085	0.606	0.0013	0.655
HPO_4^{2-}	10	0.016	0.976	0.0027	0.993
HCO_3^-	10	0.0155	0.672	0.003	0.782
$H_2PO_4^-$	10	0.0387	0.947	0.0114	0.995

Table S6 Dynamic model fitting parameters under different scavengers.

scavenger	[scavenger] (mM)	Pseudo first-order reaction		Pseudo second-order reaction	
		k_1 (min^{-1})	R^2	k_2(L·min^{-1}·mg^{-1})	R^2
Blank	0	0.0585	0.872	0.0371	0.968
BQ	0.2	0.0153	0.721	0.0025	0.76
IPA	10	0.025	0.849	0.0057	0.958
L-His	20	0.0067	0.766	0.0009	0.778
MeOH	50	0.01	0.805	0.0015	0.853
TBA	50	0.0354	0.871	0.0099	0.951

Table S7 Dynamic model fitting parameters under four cycles of $FeMoO_4$.

Number of cycles	Pseudo first-order reaction		Pseudo second-order reaction	
	k_1 (min^{-1})	R^2	k_2($L \cdot min^{-1} \cdot mg^{-1}$)	R^2
1	0.0585	0.872	0.0371	0.968
2	0.0555	0.88	0.0286	0.986
3	0.0554	0.883	0.0252	0.985
4	0.0552	0.9	0.0242	0.992

Table S8 Specific surface area, pore volume and average pore size of $FeMoO_4$, α-$FeMoO_4$, and β-$FeMoO_4$.

Sample	Surface area (m^2/g)	Pore volume (cm^3/g)	Pore size (nm)
$FeMoO_4$	18.82	0.147	31.21
α-$FeMoO_4$	8.16	0.044	21.65
β-$FeMoO_4$	3.31	0.026	30.95

Table S9 Comparison of the TC degradation effects in different reaction systems.

Catalyst	M (g/L)	C (mg/L)	T (min)	R (%)	I mg/(g·min)	System	
g-C_3N_4 /BC/Fe_2O_3	0.1	5	60	94.9	0.791	g-C_3N_4 /BC/Fe_2O_3/PDS/light	1
Bi_2WO_6/Fe_2O_3	0.33	30	30	84.8	2.57	Bi_2WO_6/Fe_2O_3/PDS/light	2
La/TiO_2 @g-C_3N_4	0.5	30	60	95.52	0.955	La/TiO_2 @g-C_3N_4/PDS/light	3
Mn–FeOOH /CNNS	0.3	20	50	99.7	1.329	Mn–FeOOH /CNNS/PDS/light	4
$MnFe_2O_4$/BC /P-CN	1	50	70	99.7	0.712	$MnFe_2O_4$/BC /P-CN/PDS/light	5
FeOOH /g-C_3N_4	0.3	20	80	98.8	0.823	FeOOH /g-C_3N_4/PDS/light	6
BiOBr	1	20	90	80.3	0.178	BiOBr/PDS/light	7
Nb_2O_5/C_3N_5	0.1	10	160	95	0.594	Nb_2O_5/C_3N_5/PDS/light	8
g-C_3N_5/BiOCl	0.3	5	90	93.7	0.174	g-C_3N_5/BiOCl/PDS/light	9
$Bi_2Fe_4O_9$/rGO /g-C_3N_4	0.2	10	40	93.8	1.173	$Bi_2Fe_4O_9$/rGO /g-C_3N_4/PDS/light	10
$ZnFe_2O_4$/Ag	0.3	20	80	90.06	0.751	$ZnFe_2O_4$/Ag/PDS/light	11
$FeMoO_4$	0.06	10	40	94.18	3.924	$FeMoO_4$/PDS/light	This paper

The variables C, R, M, and T represent the pollutant concentration (mg/L), target pollutant removal efficiency (%), catalyst dosage (g/L), and treatment time (min), respectively.

References

1 H. Yu, J. Zhang, R. Zhai, C. Gao, Y. Zhang, C. Tian and Q. Ma, Carbon, 2024, **230**, 119681.
2 W. Wang, G. Wei, Z. Fan, L. Zhang, J. Gu and F. Gao, Journal of Environmental Chemical Engineering, 2025, **13**, 116192.
3 Y. Wang, J. Xiu, T. Gan, H. Zou and F. Li, RSC Advances, 2023, **13**, 8383-8393.
4 Y. Li, C. Qu, Q. Ye, F. Meng, D. Yang and L. Wang, Environmental Research, 2024, **257**, 119293.
5 X. Liu, W. Liu, H. Zhan, X. Chen and H. Li, Solid State Sciences, 2025, **168**, 108016.
6 Y. Li, C. Qu, Q. Ye, F. Meng, D. Yang and L. Wang, Journal of Environmental Chemical Engineering, 2024, **12**, 113791.
7 Q. He, M. Ge and Q. Yu, Journal of Chemical Sciences, 2021, **133**, 98.
8 W. Liao, Z. Yang, Y. Wang, S. Li, C. Wang and Z. Zhou, Chemical Engineering Journal, 2023, **478**, 147346.
9 Y. Liu, P. Wang, C. Yin, C. Xu, X. Kang, Z. Jing, L. Chen and Z. Wang, Journal of Environmental Chemical Engineering, 2025, **13**, 115565.
10 Z. Wu, J. Shi and H. Deng, Separation and Purification Technology, 2024, **349**, 127779.
11 T. Song, X. Meng, H. Wang, C. Zhang and M. Ge, Separation and Purification Technology, 2022, **297**, 121474.